**Proceedings of the 9ICEG**
9th International Congress on Environmental Geotechnics
25-28 June, 2023 | Chania, Greece

https://doi.org/10.53243/ICEG2023-145

# Transient Analysis of Instability in Saturated Sand under Undrained Triaxial Loading Condition

Pavan Yadav[1], Viswanath Parol[2], and Amit Prashant[3]

[1]*Research Scholar, Indian Institute of Technology, Gandhinagar, India, email: yadav_pavan@iitgn.ac.in*

[2]*Assistant Professor, Department of Civil Engineering, Amrita School of Engineering, Coimbatore, Amrita Vishwa Vidyapeetham, India, email: p_viswanath@cb.amrita.edu*

[3]*Professor, Indian Institute of Technology, Gandhinagar, India, email: ap@iitgn.ac.in*

## ABSTRACT

The present study focuses on finite element analysis (FEM) of instability in saturated sands. The numerical simulation is performed under undrained conditions on the saturated triaxial specimen prepared by the moist tamping method. The differing behaviours of the granular material under steady-state and transient analysis are explored further. The steady-state analysis does not incorporate the flow of fluid in the pores of the soil sample. Whereas, the transient analysis considers the flow of pore fluid (solid-fluid diffusion) in the materials and allows the local drainage in the materials while globally remaining undrained. This study points towards the consideration of transient analysis in the simulation of saturated sand as it significantly influences the onset of instability. To simulate the nonhomogeneous sample, the density is varied along the height of the sample. The deviation in local responses for the nodes from each other is considered to identify the onset of instability. In transient analysis, it is found that the coupling mechanism between solid-fluid phases delayed the onset of instability and reduced the level of plastic deformation in the materials as compared to steady-state analysis.

*Keywords: Instability, transient analysis, steady state analysis, solid-fluid diffusion*

## 1 INTRODUCTION

In numerous experimental investigations, the instabilities are observed as localized plastic deformation forming persistent shear bands, diffused type deformation leading to solid-fluid type instability, and bulging type deformation in the specimens (Han and Vardoulakis, 1991; Desrues, 2004; Desrues and Viggiani, 2004; Khoa et al., 2006; Daouadji et al., 2011; Bhattacharya and Prashant, 2020). The origin of instability lies in the microstructure of the materials. The onset and modes of instability depend on the initial state of materials (loose or dense), type of drainage condition (drained or undrained), type of boundary constrained, type of loading path, and rate of loading (Finno et al., 1997; Desrues and Viggiani, 2004; Khoa et al., 2006; Wan et al., 2013; Mukherjee et al., 2017 & 2021). The investigations of instability are important in the geotechnical engineering practice because it (either localization or solid-fluid) is a precursor of catastrophic failure in earth structures. Various types of theories are proposed to describe and explain these phenomena, for example, bifurcation theory, equilibrium theory, and discontinuity theory (Rudnicki and Rice, 1975; Hill and Hutchinson, 1975; Leśniewska and Mróz, 2000; Borja and Lai, 2002; Regueiro and Borja, 1999; Mosler, 2004).

The onset of instability is theoretically predicted for axisymmetric conditions using bifurcation theory (Bardet and Iai, 2002; Sharma et al., 2022). Several researchers performed experimental investigations of the instability in the triaxial tests (Lade, 1982; Desrues et al., 1996; Bhattacharya and Prashant, 2020). Numerical investigations of instability in fully saturated triaxial soil specimens under undrained transient loading conditions are yet to be well understood. Leroy et al. (1990) investigated the influence of boundary conditions and geometry on the localization mode of instability in specimens under axisymmetric triaxial loading conditions. Mozaffari et al. (2022) observed a localized deformation near the end platens in the case of lubricated end boundary conditions. They observed localized deformations in the middle of the triaxial specimen in the case of nonlubricated boundary conditions. Souza (2009) observed a diffused type of deformation under drained conditions and a localized type of deformation

under undrained boundary conditions. Liu et al. (2004) numerically illustrated the mechanism of strain localization in the fully saturated 3D sand specimen under true triaxial loading conditions. They observed that permeability, geometry, and drainage conditions significantly influence the initiation and development of localized deformation. Reduced plastic deformation in the shear band and delayed onset of localization was observed with a decrease in the permeability value. Further, various types of shear bands were observed for different types of specimen geometry. In undrained boundary conditions, localized deformation was observed at a higher strain level as compared to drained boundary conditions. Wan et al. (2013) performed numerical simulation on the triaxial test with coupled solids-fluids interaction analysis and observed shear band passing through the soil specimen diagonally. Further, it was observed that the type of loading path affects the onset of instability in the materials. Delayed onset of instability was depicted in the constant shear (CSD) test as compared to the quasi-constant shear undrained (QCSU) test.

The present study focuses on the numerical investigation of the instability in the fluid-saturated sands by a finite element tool, namely ABAQUS v6.14. In this numerical investigation, a fully saturated sand specimen under triaxial loading conditions with transient analysis is considered. The significance of fluid flow on the onset of instability and magnitude of plastic deformation is explored by a comparative study between steady-state analysis and transient analysis.

## 2 CONSTITUTIVE MODEL AND PREDICTION OF STRESS –STRAIN RESPONSE OF SAND

The response of the material has been characterized by the Modified Drucker-Prager/Cap plasticity model. The yield surface of the cap model consists of two different surfaces: one is the shear failure surface, and another one is the cap surface for considering the failure due to volumetric strain accumulation. There is a transition surface between these two surfaces. The shear failure surface allows the shear flow while the cap controls the increase in volumetric strain during the shear yielding. Cap also provides the plastic hardening behaviour of the material. In the cap zone, the model provides plastic flow as associative. However, in the transition and shear zone, the plastic flow is non-associative (ABAQUS, 2014).

The yield surface of the cap model consists of three different surfaces as follows.
Drucker-Prager failure surface is considered as the shearing yield surface:

$$f_s = q - Mp' - d \tag{1}$$

Where $q$ and $p'$ are effective shear stress and effective mean pressure. $M$ is the stress ratio at a critical state.
The cap yield surface is defined as:

$$f_v = \sqrt{((p' - p'_a)^2 + (Rq/(1 + \alpha - \alpha/cos\beta))^2)} - R(d + p'_a M) \tag{2}$$

Where $\alpha$ and $R$ are material parameters. $M = tan\beta = 6sin\varphi'/(3 - sin\varphi')$ and $d = 18c'cos\varphi'/(3 - sin\varphi')$. Here, $c'$ and $\varphi'$ are shear strength parameters.

And,
$$p'_a = (p'_b - Rd)/(1 + RM) \tag{3}$$

Where $p'_a$ is defined as the evolution parameter defining the softening/hardening behaviour due to plastic volumetric strain. $p'_b$ is the hydrostatic compression yield stress. The softening/hardening response of the cap model is implemented as user-defined and can be calculated using the following relationship between $p'_b$ and plastic volumetric strain ($\varepsilon_v^p$).

$$\varepsilon_v^p = \int d\varepsilon_v^p = ((\lambda - \kappa)/(1 + e)) \int (dp'_b/p'_b) \tag{4}$$

Where $\lambda$ and $\kappa$ are material parameters and $e$ is the void ratio.
The transition yield surface between the above two surfaces is defined in equation (5):

$$f_t = \sqrt{((p' - p'_a)^2 + (q - (1 - \alpha/cos\beta)(d + p'_a M))^2)} - R(d + p'_a M) \tag{5}$$

An associative flow rule is considered for the cap, and a non-associative flow rule is adopted for the transition surface and shear surface having the same plastic potential surface as mentioned below.

$$g_t = g_s = \sqrt{\left((p' - p'_a)M\right)^2 + (q/(1 + \alpha - \alpha/cos\beta))^2} \quad (6)$$

The material parameters have been calibrated for the sand, and the stress-strain response has been predicted under triaxial loading conditions. The schematic diagram of the triaxial test with appropriate boundary and loading conditions is described in Figure 1(a). The simulations were performed in two steps. Initially, the geostatic condition was applied to attain the effect of initial confining pressure, and later, the strain-controlled loading condition was enforced at the top boundary for shearing the specimen. The material parameters adopted for analysis are listed in Table 1. A set of simulations were carried out on a single finite element to capture and verify the response of the material at varying confining pressure (20, 50, and 100kPa). CAX8R (8-node biquadratic, reduced integration plane strain element) type element was adopted in the current numerical simulation.

**Table 1.** *Material parameters adopted in numerical analysis*

| Material parameters | Value |
|---|---|
| Logarithmic bulk modulus, k | 0.0034 |
| Slope of isotropic consolidation line, λ | 0.02 |
| Poisson's ratio, v | 0.3 |
| Material cohesion, d (kPa) | 0.1 |
| Angle of friction, $\beta^0$ | 52 |
| Transition surface parameter, α | 0.01 |
| Cap eccentricity, R | 1.25 |
| Flow stress ratio, K | 1 |

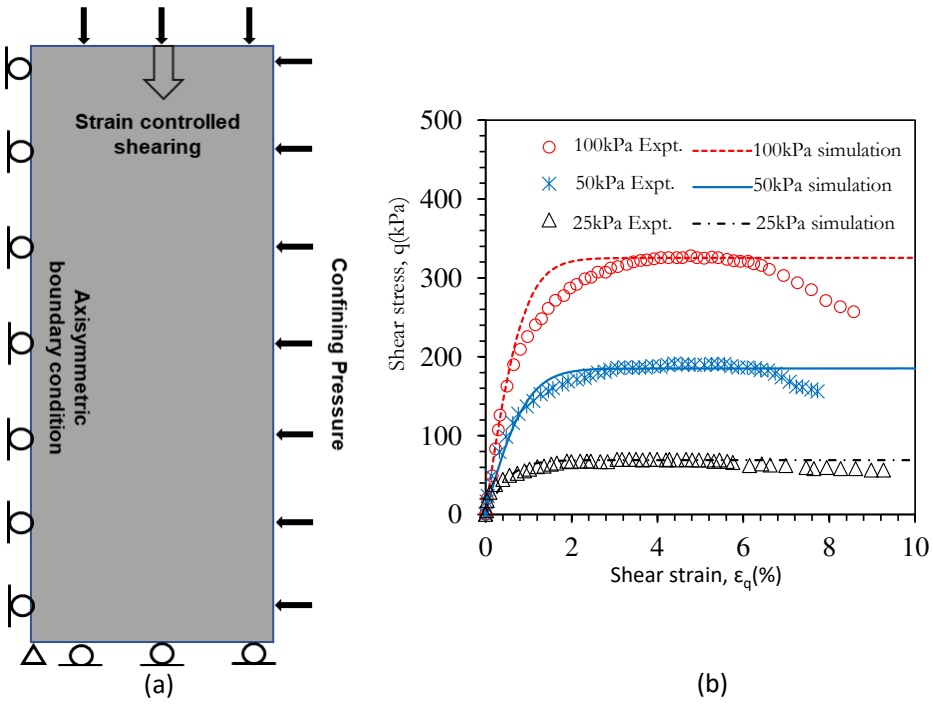


***Figure 1.*** *(a)Schematic diagram of triaxial test simulation in ABAQUS (b) Predicted and experimental (Lee, 2000) stress-strain responses at different confining pressures.*

The experimental observations by Lee (2000) are used to validate the simulation with axisymmetric boundary conditions and were found reasonable, except for the mismatch at high plastic strains (Figure 1(b)) that occur after the potentially evolved instabilities in the specimen. The reason is the inadequacy of the inbuilt material model in the ABAQUS to capture the softening response of the material.

## 3 RESULTS AND DISCUSSIONS

### 3.1 Simulation details

An axisymmetric triaxial sand specimen with a height of 100mm and a diameter of 50mm is used for analysis. The bottom surface is restrained in the vertical and radial directions. Initial confining pressure of 100kPa is applied to the specimen. During the shearing stage, a deformation rate of 0.1 mm/min is applied at the top surface, as shown in Figure 2. The specimen is discretized into 3360 elements with a 20-node brick with pore pressure, quadratic displacement, linear pore pressure, and reduced integration (C3D20RP) type element for simulating coupled pore pressure-deformation analysis. The specimen is divided into 4 layers having different void ratios (increasing from bottom to top) to mimic the soil sample prepared by the moist temping method (Hu et al., 2006). While other parameters were assumed to be constant for each layer (Table 1). A full Newton-Rapshon iteration technique with an unsymmetric equation solver has been used to solve the equilibrium equation.

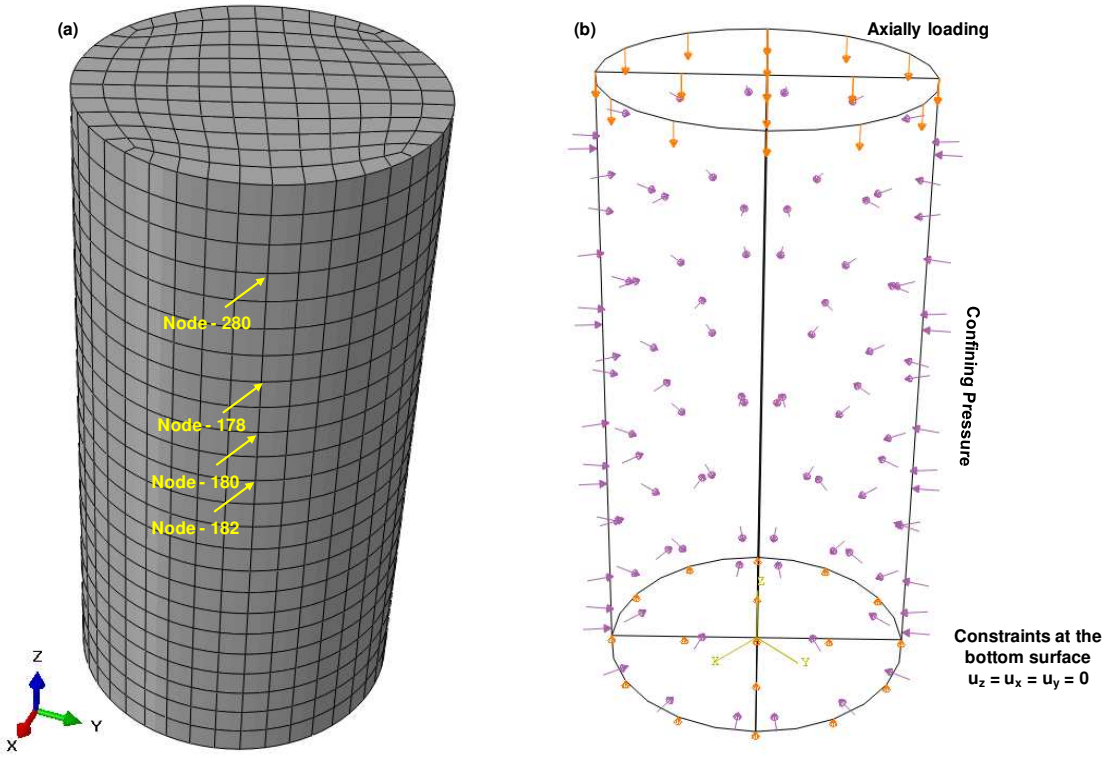


***Figure 2**. Axisymmetric triaxial specimen with (a) mesh (b) applied boundary conditions*

### 3.2 Undrained transient analysis

The conventional undrained triaxial compression test is simulated in two steps on the soil specimen prepared by the moist tamping method. The water within the pores of sand is free to flow within the saturated sample, which creates a locally drained condition. The flow of water follows the generalized Darcy's law (or Forchheimer's equation) and satisfies the equation of continuity (ABAQUS, 2014). The mesh of the fluid (water) phase is connected with the mesh of the solid phase and the water is allowed to flow through the meshes. The sample's boundaries are made impermeable, creating the undrained condition. Hence, this creates a locally drained and globally undrained situation. A transient coupled pore pressure/ effective stress analysis backward difference operator is used to integrate the continuity equation. An unsymmetric solver is used for convergence (ABAQUS, 2014). The simulation was carried out until the shear strain accumulation reached 20%.

The numerically simulated results are presented in Figures 3 and 4 for undrained triaxial loading conditions. The contour of the magnitude of plastic strain (PEMAG = $\varepsilon_m^{pl} = \sqrt{((2/3) * (\varepsilon_1^p \varepsilon_1^p + \varepsilon_2^p \varepsilon_2^p + \varepsilon_3^p \varepsilon_3^p))}$ ) is plotted on the final deformed configuration of the specimen. A dominant zone of localized deformations forming a persistent shear band was clearly observed passing diagonally through the soil specimen. The maximum magnitude of plastic strain (PEMAG) is identified in the shear band as compared to other parts of the sand specimen. A tilted shape of a triaxial specimen and nonhomogeneous plastic deformation is observed, as depicted in Figure 3. A similar type of deformed shape of the sand specimen was experimentally observed by Hu et al. (2006) in their conventional triaxial compression (CTC) test. The positions of the node are marked in Figure 2. Node-180 lies in the centre of the localized zone, and node-280 lies far away from the localized zone. The other two nodes (178 and 182) lie near the shear band. Local deviatoric stress versus global axial strain is plotted for these four different nodes in Figure 4(a). It is observed that at 1.58% global axial strain ($\varepsilon_a$), the local deviatoric stress response of all four nodes starts to deviate suddenly from each other. The sudden deviation in the deviatoric stress response is a distinct indication of the onset of localized deformation in the materials Figure 4(a). In this numerical study, the local variation of the response is considered the onset of instability in the material. However, it has been observed by researchers that the global stress-

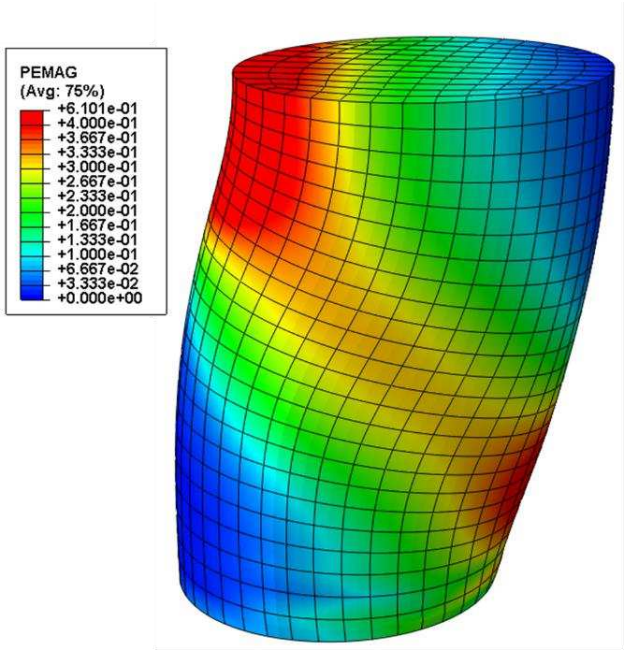


***Figure 3.*** *Contour of magnitude of plastic strains (PEMAGs) on final deformed configuration*

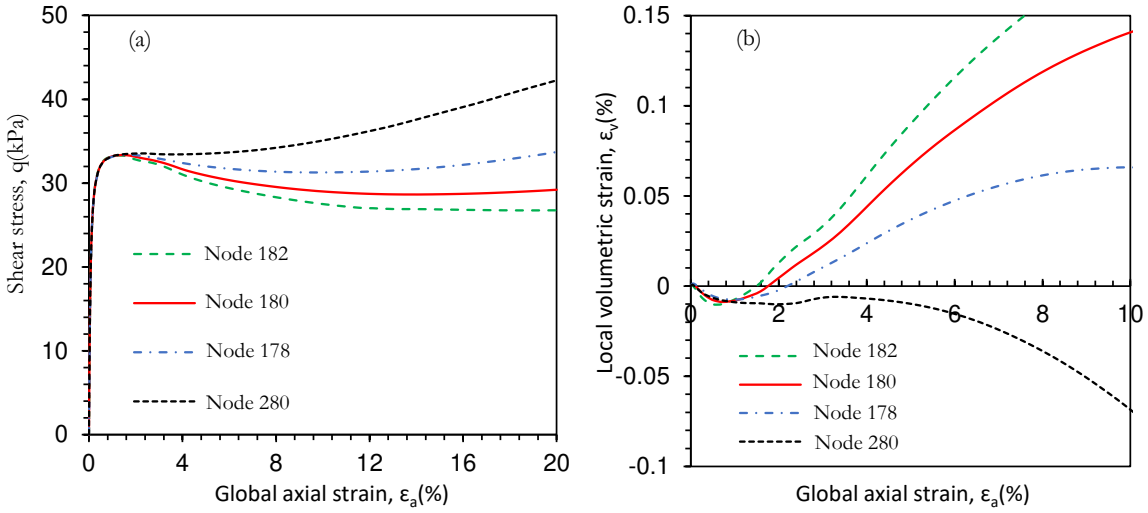


***Figure 4****. Evolution of (a) local deviatoric stress with global axial strain (b) local volumetric strain with global axial strain, at marked nodes*

strain response approach overpredicts the onset of localization (Mukherjee et al., 2021). Local volumetric strain response is plotted against global axial strain for node-180 (inside the shear band) and node -280 (far away from the shear band) in Figure 4(b). The material inside and outside the shear band observes a contractive type response (local $d\varepsilon_v < 0$) up to the point of instability ($\varepsilon_a$ = 1.58%). On further shearing, the material outside the shear band observes a continuously contractive type response, while the material inside the shear band starts to observe a dilative type response (local $d\varepsilon_v > 0$).

### 3.3 Effect of steady state and transient analysis on the instability

To get a better understanding of the impact of steady state and transient analysis on instability, separate analyses were carried out. For both analyses, the procedure remains the same for the consolidation stage. But in the shearing stage, steady state and transient condition were used. The steady-state coupled pore pressure/ effective stress analysis assumed that there is no transient effect in the continuity equation. The unsymmetric matrix solution and storage scheme are used automatically for steady-state analysis steps. Undrained boundary conditions are applied on the top and bottom surfaces. The contours of the magnitude of plastic strains (PEMAGs) are plotted on the undeformed shape of the specimen, as shown in Figure 5(a).

In steady-state analysis, two shear bands clearly appeared in the bottom region of the specimen. These shear bands propagate from bottom corners and nucleate in a particular zone during shearing (Figure 5(a)). While in transient analysis, a single shear band appears, crossing through the specimen diagonally (Figure 5(b)). In the steady-state analysis, the accumulated plastic strain in the localized zone is higher than in the transient analysis. In the shear band, the maximum observed PEMAGs is 0.711 and 0.610 for steady-state and transient analysis. A reduction of 0.101 in PEMAG can be observed for transient analysis as compared to steady-state analysis. The orientation angle ($\theta_s$) of the shear band appears at $47^0$ and $49^0$ in the case of steady-state analysis and transient analysis, respectively. Further, the width of the localized zone is approximately measured as 2.76 mm and 16.26 mm for steady state and transient analysis. The positions of nodes are marked in Figure 5. Nodes 353 and 3 lie inside the localized zone, while nodes 351 and 45 lie outside the localized zone for steady state and transient analysis. In Figures 6(a) and 6(b), the local plastic strains (PEMAGs) are plotted against the global axial strain ($\varepsilon_a$) for both steady-state analysis and transient analysis. The sudden deviation in the local magnitude of plastic strain for the node in the shear band indicates a bifurcation point. The initiation of localized deformation appears at around 1% global axial strain ($\varepsilon_a$) steady-state analysis (Figure 6(a)).

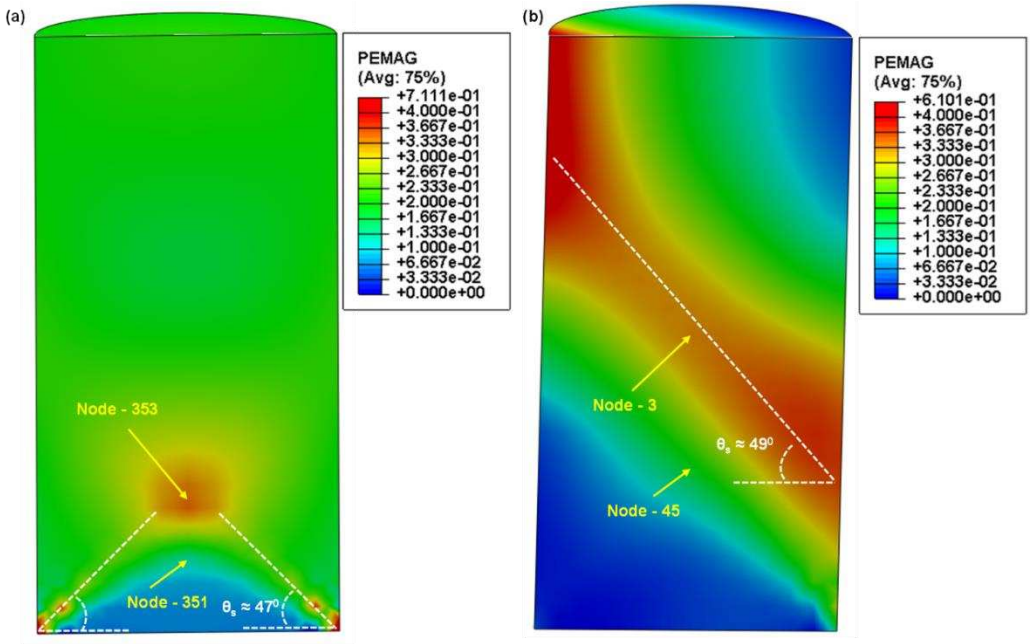


***Figure 5****. Contour of the magnitude of plastic strains (PEMAGs) on undeformed configuration for (a) steady state analysis (b) transient analysis*

However, in the case of transient analysis, delayed onset of localization (at 1.58% global axial strain, $\varepsilon_a$) is observed as compared to steady-state analysis (Figure 6(b)). The delayed onset of instability and lower magnitude of plastic strain (PEMAG) can be observed in the case of transient analysis due to the coupling mechanism between solid and fluid phases. This mechanism plays a significant role in the onset of instability and plastic deformation in the materials. In transient analysis, the fluid initially takes the load, and slowly the load is transferred to the soil's solid skeleton. However, in steady-state analysis, there is no coupling mechanism between solid and fluid, and the applied load is directly taken by the solid skeleton.

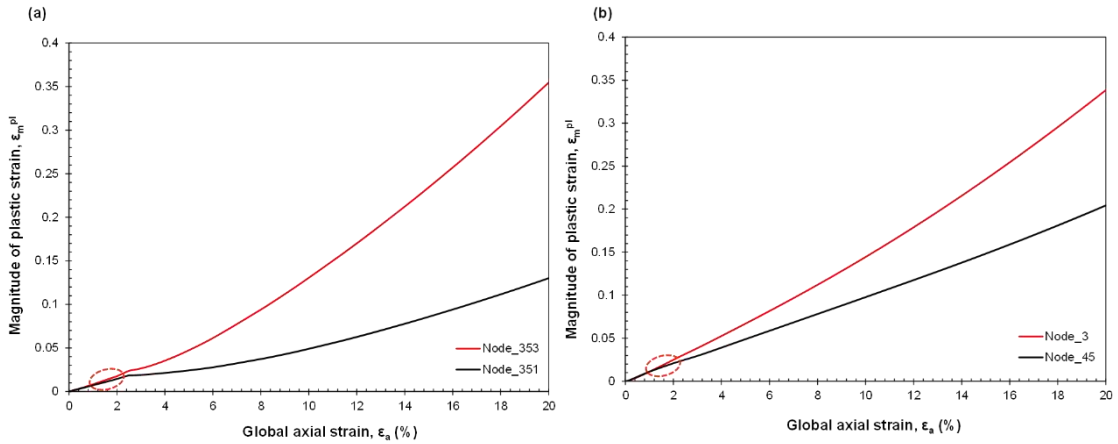


***Figure 6**. Evolution of local magnitude of plastic strain with global axial strain at marked nodes for (a) steady state analysis (Nodes – 351 & 353) (b) transient analysis (Nodes 3 & 45)*

## 4 CONCLUSIONS

The response of sand specimens under undrained transient loading conditions was explored in detail in the present study. The sand specimen was prepared in 4 layers with different void ratios to mimic the moist tamping method of sample preparation. The predicted stress-strain responses at different confining pressure were in good agreement with the experimental results, except for capturing the softening response of the soils after potential instabilities. The sudden variation in the local responses is considered an indication of the onset of localized deformation in the numerical framework. In transient analysis, a single shear band was observed, while an inverted V-shaped shear band was observed in the steady-state analysis. The steady-state analysis does not encounter the effect of fluid flow into the materials and pore pressure issues. However, transient analysis encounters all these issues. In transient analysis, It is found that the coupling mechanism between soil solid and fluid delayed the onset of bifurcation and reduced the level of plastic deformation in the localized zone. Hence, for accurate prediction of instability and for the actual response of soil, a transient analysis needs to be performed.

## REFERENCES

Abaqus, S., Fallis, A. D. S., & Techniques, D. (2014). ABAQUS analysis user's guide (6.14). *Dassault Systemes Simulia Corp., Providence*.

Bardet, J. P., & Iai, S. (2002). Axisymmetric instability of fluid saturated pervious cylinders. *J. Appl. Mech.*, *69*(6), 717-723.

Bhattacharya, D., & Prashant, A. (2020). Effect of loading boundary conditions in plane strain mechanical response and local deformations in sand specimens. *Journal of Geotechnical and Geoenvironmental Engineering*, *146*(9), 04020086.

Borja, R. I., & Lai, T. Y. (2002). Propagation of localization instability under active and passive loading. *Journal of geotechnical and geoenvironmental engineering*, *128*(1), 64-75.

Daouadji, A., Darve, F., Al Gali, H., Hicher, P. Y., Laouafa, F., Lignon, S., & Wan, R. (2011). Diffuse failure in geomaterials: experiments, theory and modelling. *International Journal for Numerical and Analytical Methods in Geomechanics*, *35*(16), 1731-1773.

de Souza, M. P. (2009). Constitutive and computational aspects of localized and diffuse instabilities in geomaterials. University of Calgary, Department of Civil Engineering.

Desrues, J. (2004). Tracking strain localization in geomaterials using computerized tomography. *X-ray CT for Geomaterials*, 15-41.

Desrues, J., Chambon, R., Mokni, M., & Mazerolle, F. (1996). Void ratio evolution inside shear bands in triaxial sand specimens studied by computed tomography. *Géotechnique*, *46*(3), 529-546.

Desrues, J., & Viggiani, G. (2004). Strain localization in sand: an overview of the experimental results obtained in Grenoble using stereophotogrammetry. *International journal for numerical and analytical methods in geomechanics*, *28*(4), 279-321.

Finno, R. J., Harris, W. W., Mooney, M. A., & Viggiani, G. (1997). Shear bands in plane strain compression of loose sand. *Geotechnique*, *47*(1), 149-165.

Han, C., & Vardoulakis, I. G. (1991). Plane-strain compression experiments on water-saturated fine-grained sand. *Geotechnique*, *41*(1), 49-78.

Hill, R., & Hutchinson, J. W. (1975). Bifurcation phenomena in the plane tension test. *Journal of the Mechanics and Physics of Solids*, *23*(4-5), 239-264.

Hu, C., Ng, T. T., & Altobelli, S. (2006). Void distributions in samples of Ottawa sand. *Geomechanics and Geoengineering: An International Journal*, *1*(3), 197-206.

Khoa, H. D. V., Georgopoulos, I. O., Darve, F., & Laouafa, F. (2006). Diffuse failure in geomaterials: Experiments and modelling. *Computers and Geotechnics*, *33*(1), 1-14.

Lade, P. V. (1982). Localization effects in triaxial tests on sand.

Lee, W. F. (2000). Internal stability analyses of geosynthetic reinforced retaining walls. University of Washington.

Leroy, Y., & Ortiz, M. (1990). Finite element analysis of transient strain localization phenomena in frictional solids. *International Journal for Numerical and Analytical Methods in Geomechanics*, *14*(2), 93-124.

Leśniewska, D., & Mróz, Z. (2000). Limit equilibrium approach to study the evolution of shear band systems in soils. *Geotechnique*, *50*(5), 521-536.

Liu, X., Scarpas, A., & Blaauwendraad, J. (2005). Numerical modelling of nonlinear response of soil. Part 2: Strain localization investigation on sand. *International journal of solids and structures*, *42*(7), 1883-1907.

Mosler, J. (2004). On the modeling of highly localized deformations induced by material failure: The strong discontinuity approach. *Archives of Computational Methods in Engineering*, *11*, 389-446.

Mozaffari, M., Liu, W., & Ghafghazi, M. (2022). Influence of specimen nonuniformity and end restraint conditions on drained triaxial compression test results in sand. *Canadian Geotechnical Journal*, *59*(8), 1414-1426.

Mukherjee, M., Gupta, A., & Prashant, A. (2017). Instability analysis of sand under undrained biaxial loading with rigid and flexible boundary. *International Journal of Geomechanics*, *17*(1), 04016042.

Mukherjee, M., Gupta, A., & Prashant, A. (2021). A rate-dependent model for sand to predict constitutive response and instability onset. *Acta Geotechnica*, *16*, 93-111.

Regueiro, R. A., & Borja, R. I. (1999). A finite element model of localized deformation in frictional materials taking a strong discontinuity approach. *Finite Elements in Analysis and Design*, *33*(4), 283-315.

Rudnicki, J. W., & Rice, J. R. (1975). Conditions for the localization of deformation in pressure-sensitive dilatant materials. *Journal of the Mechanics and Physics of Solids*, *23*(6), 371-394.

Sharma, S., Parol, V., & Prashant, A. (2022, July). Liquefaction instability analysis using extended Mohr-Coulomb model under axisymmetric conditions. In *Challenges and Innovations in Geomechanics: Proceedings of the 16th International Conference of IACMAG-Volume 3* (pp. 134-141). Cham: Springer International Publishing.

Wan, R., Pinheiro, M., Daouadji, A., Jrad, M., & Darve, F. (2013). Diffuse instabilities with transition to localization in loose granular materials. *International Journal for Numerical and Analytical Methods in Geomechanics*, *37*(10), 1292-1311.